Dual-Patch Polarization Conversion Metasurface-Based Wideband Circular Polarization Slot Antenna

QIANG CHEN AND HOU ZHANG

Air-Defense and Antimissile Institute, Air Force Engineering University, Xi'an 710051, China

1Corresponding author: Qiang Chen (1062620145@qq.com)

ABSTRACT In this paper, a novel polarization conversion (PC) structure is introduced, and its use with a wideband, wide 3-dB axial-ratio (AR) beam, low-radar-cross-section (RCS) circular polarization (CP) slot antenna is suggested. The unit cell of the proposed PC metasurface (PCM) consists of square and L-shaped patches separated by an L-shaped slot printed on an FR4 substrate. The mechanisms for linear to circular polarization and bandwidth improvement of a conventional antenna are analyzed theoretically. Through numerical optimizations and parametric studies, a simulated 10-dB impedance bandwidth of 42.7% (4.15–6.4 GHz) and a 3-dB AR bandwidth of 26.2% (4.8–6.25 GHz) are achieved by the proposed antenna. As the simulation demonstrates, the proposed antenna achieves an average 20-dB RCS reduction in a wide band from 5.25 to 6.8 GHz compared with a conventional slot antenna covered by the PC band. In addition, compared with the previously reported work, the PCM-based CP antenna exhibits a larger 3-dB AR beam width of 200° in the *xoz* plane and 120° in the *yoz* plane, and a wider CP bandwidth within the operational bandwidth. Finally, an overall volume of $0.55\lambda_0 \times 0.55\lambda_0 \times 0.05\lambda_0$ centered at 5.275 GHz is fabricated and measured, demonstrating good agreement with the simulation results.

INDEX TERMS Polarization conversion metasurface, circularly polarized, dual-patch, low RCS.

I. INTRODUCTION

Metamaterials, including frequency-selective surfaces, metasurfaces, artificial magnetic conductors (AMCs), left-handed materials, and electromagnetic band-gap structures, are widely described as inhomogeneous or inartificially homogeneous electromagnetic structures owing to their distinctive characteristics [1], [2]. Specifically, a pivotal use for a two-dimensional metamaterial, polarization conversion (PC), can obtain circularly polarized waves from linearly polarized waves [3], [4]. For instance, by utilizing a metallic two-dimensional metamaterial [5], theoretical explanations for polarization rotation from a linearly polarized state to circularly polarized waves were demonstrated by Silveirinha. However, due to the large size of the spatial three-dimensional configuration, this design may not be applied to low-profile configurations. Many planar two-dimensional metamaterials (MSs) have been designed to realize the polarization rotation from a linear to a circularly polarized state [2], [6], [7]. Owing to the twist structures obtained by rotating the MS units, most can realize the polarization change.

MSs have been applied to realize enhancements in bandwidth and an overall reduction for various antenna designs [8]–[11]. For instance, in our prior research, a 4 × 4-array mushroom antenna combined with an L-shaped slot antenna fed by CP waves was engineered to obtain wideband CP radiation and high-gain performance. Specifically, by utilizing planar two-dimensional MMTs (MSs) as the superstrate covering on a conventional microstrip slot antenna, a wideband, low-profile, high-gain CP antenna was possibly obtained in recently reported designs [12]–[14]. A design was demonstrated in which polarization rotation from a linear to a circular polarization state was achieved using MS [15]. However, the application cannot be achieved with a low-profile and size-reducing design because an air layer separating the source antenna and the MS increases the thickness of the design antenna. Another compact design without an air gap with polarization-dependent performance was proposed by utilizing a corner-truncated square MS as the superstrate, but the AR bandwidth was narrow compared to that of the reported antenna [16].

Thus, enhancements in AR bandwidth and size reduction are still challenging, and many studies continue to be conducted [17]–[20]. Unfortunately, many designs make minor contributions in terms of wide CP radiation bandwidth, wide AR beam width, and low RCS. Different from a conventional single-feed patch antenna or dual/multi-feed antenna with a complex feeding network design, a PCM structure as the superstrate of a single-feed slot antenna exhibits a wide impedance-matching band, a wide 3-dB AR bandwidth, and a wide CP operation band. In particular, in previous work [21], an MS-based slot structure utilizing a corner-truncated square cell, whose AR bandwidth was greater than 18%, was proposed for CP. However, there is still significant room to improve the performance in terms of low profile, low RCS, and wider AR bandwidth. Nevertheless, a good CP property can be obtained by a PCM-based antenna with a slot structure.

In the work described in this paper, a planar PCM structure based on a dual-patch MS is utilized to realize polarization conversion, and then, as an application, a slot antenna covered by the proposed PCM structure is designed. The designed low-profile CP slot antenna achieves a wide impedance bandwidth, wide 3-dB AR beam width, and low RCS. Compared to recently reported designs, a dual-patch MS is used to improve the design flexibility by altering the *L*-shaped slot size and cell spacing to achieve a wider CP operating bandwidth and wider AR beam width. Comparable size characteristics, matching bandwidth, wide impedance, the largest AR beam width, and a wider CP operation band are achieved by the proposed antenna. In particular, a larger 3-dB AR beam width of 200° in the *xoz* plane and 120° in the *yoz* plane can be attained, and an average 100° beam width in two planes can be achieved.

II. ANTENNA CONFIGURATION AND ANALYSIS

A. ANTENNA CONFIGURATION

Fig. 1 presents the proposed dual-patch AMC-based planar PC structure and slot-feeding structure. In particular, the CP antenna is composed of three layers. The top layer comprises

an array arranged in a 4×4 layout using a dual-patch AMC-based PC metasurface cell with periodicity W that is printed on the top side of an FR4 substrate ($\varepsilon_r = 4.4$ and $\tan \delta = 0.02$). The middle layer is an air slot etched on the metallic ground. A conventional slot antenna is constructed for coupling energy to the PCM structure. The strip-feeding line on the bottom layer is used to excite the slot antenna to radiate properly, and is connected to the middle layer by a metallic layer via loading in the wider-width sides of the feeding line for impedance-matching in the lower-pass band. The middle and bottom layers are separated by a Rogers RO3003™ substrate with a dielectric constant $\varepsilon_r = 3$ and $\tan \delta = 0.0013$, with a thickness of $h_1 = 0.5$ mm. It should be noted that between such a PCM and slot antenna there is no air gap, while the same ground plane is shared. Thus, a low-profile antenna can be realized by this design. The parameter definitions for each functional layer are found in Figs. 1(a) and 1(b), and the optimized dimensions are provided in the caption.

An MS cell for linear-to-circular polarization using the proposed dual-patch AMC structure is presented in Fig. 1. Fig. 1(a) shows that the AMC-based PCM unit cell has an *L*-shaped square metal patch, separated by an *L*-shaped slot with widths V_x, V_y and distances from center of substrate P_x, P_y. It is put on the upper sides of a dielectric slab of FR4 with a thickness of $0.05\lambda_0$ at 5.275 GHz.
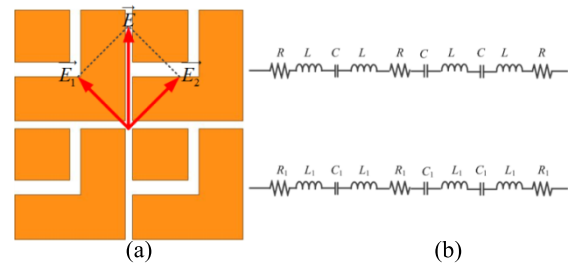
FIGURE 2. (a) Mechanism of producing CP waves via an LP wave for dual-patch MS; (b) Equivalent circuit.

B. MECHANISM OF CIRCULAR POLARIZATION

To schematically explain the mechanism of generating circularly polarized radiation from a slot antenna for a linearly polarized (LP) state based on a dual-patch MS, similar to a previous explanation [21], an equivalent mode is given, as shown in Fig. 2. Here, for clarity, as seen in Fig. 2, the LP wave radiating from the slot antenna (electrical field $\vec{E}$ in the *x* direction) may be fixed into two orthogonal components ($\vec{E_1}$ and $\vec{E_2}$. As two such electrical fields go through an MS, the electromagnetic (EM) waves will interface with the MS, and this type of mutual interface can be expressed by the impedance equation

$$\left(R_i + 1/(jwC_i) + jwL_i\right) I_i = \sum\nolimits_i \quad (i = 1, 2), \quad (1)$$

where R_i, C_i, and L_i are the resistances and inductances for both categories of patches in two orthogonal directions, and
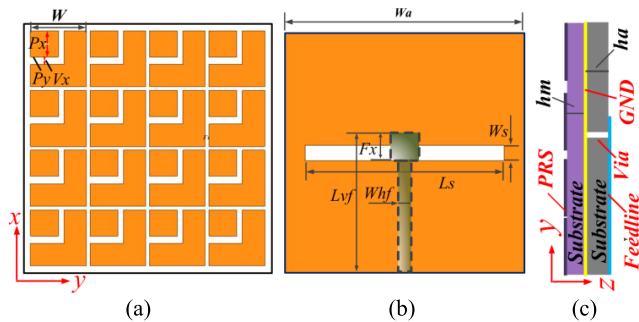
FIGURE 1. (a) Configuration of dual-patch MS superstrate slot antenna; (b) Top and bottom views of slot antenna; (c) Pictures of produced dual-patch superstrate slot antenna. Dimensions are $V_x = V_y = 1.5$, $G = 0.5$, $W = 8$, $W_a = 33.5$, $P_x = P_y = 0.75$, $ha = 0.5$, $d = 0.5$, $hm = 2.4$, $F_{lx} = 6$, $F_{ly} = 14$, $W_{hf} = 1.6$, $L_{vf} = 19.5$, $F_x = 3.8$, $L_s = 28$, and $W_s = 2.2$ (all in mm).

$\sum_i$ is the external excitation correlated with the produced EM fields from the slot antenna separated uniformly by the two parts. Owing to the gap between adjacent and different patch dimensions, the values of R_i, C_i, and L_i will differ, resulting in different values of induced currents I_i. After that, the radiation fields from the MS in the two corresponding directions will vary.

As expressed by the impedance equation, when the dual-patch PCM design satisfies $|Z_1| = |Z_2|$ and $\text{ang}(Z_1 - Z_2) = \pm 90°$, CP radiation will be obtained. In this design, owing to the different widths etched between the L-shaped slot and the square patch of the MS, the phase of $\vec{E}_1$ is obviously ahead of that of $\vec{E}_2$, and left-hand CP (LHCP) is achieved. A similar analysis of the mechanism was given by Zhu *et al.* [15]. Hence, right-hand CP (RHCP)/LHCP can be generated by adjusting the dimension of dual-patch MS cells, such that $|Z_1| = |Z_2|$ and $\text{ang}(Z_1 - Z_2) = \pm 90°$:

$$Z_i = R_i + 1/(jwC_i) + jwL_i \quad (i = 1, 2). \quad (2)$$

Based on the prior detailed theoretical evaluation, to achieve good CP radiation, we performed co-optimizations for the slot antenna covered by a dual-patch MS. For the optimized antenna, to achieve a wide operating bandwidth, the MS should have equivalent operating frequency bands to the slot antenna. Therefore, to achieve a broad impedance-matching bandwidth and AR bandwidth, the designed antenna should be carefully optimized. The impacts of certain parameters are revealed by the numerical performance of the structural parametric studies.
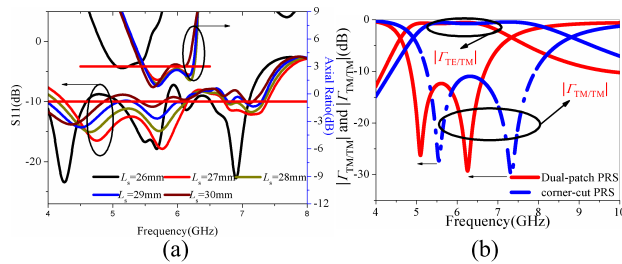

FIGURE 3. (a) S_{11} and AR with different slot lengths L_S; (b) Magnitudes of reflection coefficients. $\Gamma_{TE/TM}$ and $\Gamma_{TE/TM}$ of corner-cut PRS and dual-patch PRS [21].

As shown in Fig. 3(a), as the slot length L_S of the slot antenna increased, the impedance-matching band shifted to a lower frequency, albeit via a narrower bandwidth. This frequency shift appears mainly due to the decreasing magnetic flow path within the slot. The narrower bandwidth is due to the impedance mismatching of the entire antenna structure. The L_S value will also affect the AR property, including the minimum AR frequency points and bandwidth. It can be seen that the second minimum AR frequency point shifted to a lower AR value when the slot length L_S increased within the range. However, a gap will be noted in a big AR band where a division into a couple of separating AR bands occurred once the length slot L_S continued to increase, causing a narrower AR width. We also investigated the effect of the
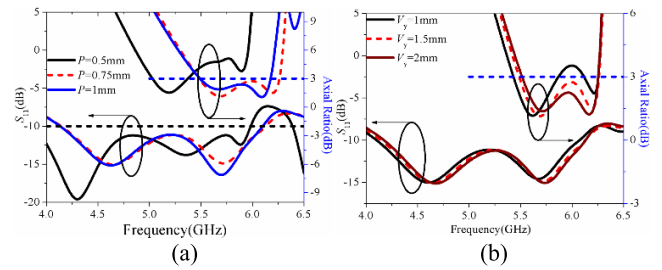

FIGURE 4. S_{11} and AR with different widths of L-shaped slots and distances to the center of MS unit: (a) Distance to center, P; (b) Width of L-shaped slot, V_Y.

MS unit size, unit spacing, and L-shaped slot on antenna performance, especially the AR property. We performed a parametric study on the L-shaped slot, and, as illustrated in Fig. 4, an increased length of the L-shaped slot of the dual-patch MS will improve the AR bandwidth, while having little impact on the impedance bandwidth.
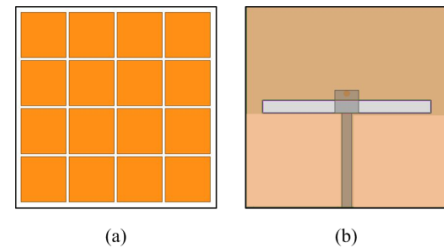

FIGURE 5. Configuration of reference LP slot antenna: (a) MS without L-shaped slot; (b) Feeding structure.
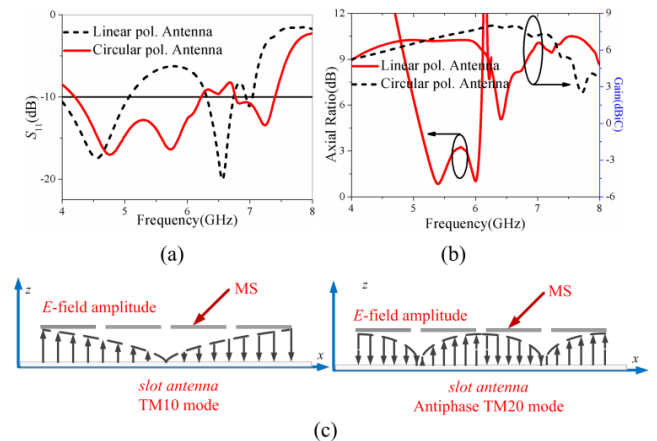

FIGURE 6. Simulated results for reference LP and CP antennas: (a) S_{11} and (b) Radiation gain and AR; (c) Diagram of two resonance modes.

To compare with the proposed antenna, Fig. 5 presents the S_{11}, axial ratio and radiation gain of the correlating LP antenna covered by the MS without an L-shaped slot. It can be seen in Fig. 6(c) that there are two resonance modes, a typical TM10 mode and an antiphase TM20 mode, occurring in both the reference antenna and proposed antenna. Then a broad
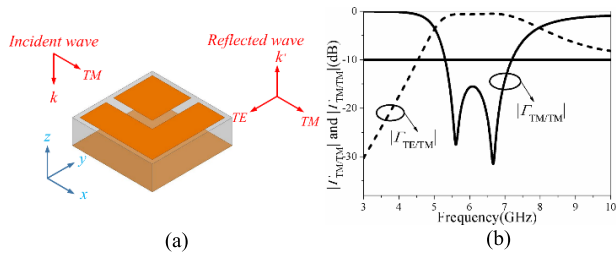
FIGURE 7. (a) Simulation model. (b) Co- and cross-polarization reflections of MS.

FIGURE 9. Simulated angular dependence of AR in the xoz and yoz planes at (a) 5.6 and (b) 6.2 GHz.

impedance bandwidth can be achieved, since the two resonance modes are near to each other for the CP antenna. Thus, for the separated bandwidth of the LP antenna, the impedance bandwidth is increased, with a fractional bandwidth of 42.7% (4.15-6.4 GHz). As shown in Fig. 5(b), there is a slight gain drop in the CP antenna, in particular at the higher frequency, but the gain remains larger than 3.5 dB. As can be seen, due to the large AR value of the LP antenna, the AR curve cannot be observed in the figure, but the proposed CP antenna exhibits good CP radiation.
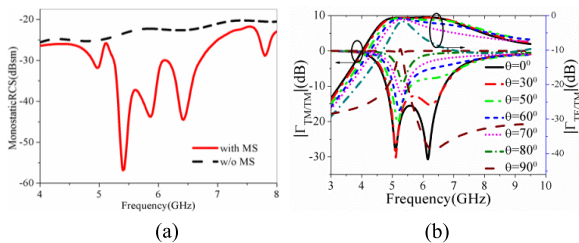

FIGURE 8. (a) Simulated RCS of proposed antenna compared with that of slot antenna without MS under normal-incidence wave parallel to x axis. (b) Magnitudes of reflection coefficients in case of TM oblique incident waves.

C. RCS REDUCTION MECHANISM

To comprehend the physical mechanism of RCS reduction, the qualities of the MS unit cell were examined in simulation. Ansoft's HFSS was utilized to examine the suggested PRS's reflection qualities using the Floquet-port model. The transverse-electric (TE) and -magnetic (TM) waves show a linearly polarized property but are orthogonal. As shown in Fig. 8(a), as a TM-polarized typical incident wave with an electric field in the x direction is reflected by the unit cell, the TM- and TE-polarized waves are reflected. Since the incident angle is equivalent to $0°$, the TE mode of the complete broadside radiation is just about equivalent in amplitude, but it has a $90°$ phase variation to the TM modes. After that, $\Gamma_{TE/TM}$ shows the ratio of an orthogonal TE-reflected electric field to the TM incident electric field. It can be seen in Fig. 8(b) that $\Gamma_{TE/TM}$ is less than -10 dB, while $\Gamma_{TM/TM}$ is nearly 0 dB, covering the bandwidth from 5 to 7.5 GHz. This indicates that the designed MS is capable of converting the x-polarized incident wave to its orthogonal direction in a wide band. Therefore, as demonstrated in Fig. 9, the RCS of the proposed antenna is significantly reduced along the
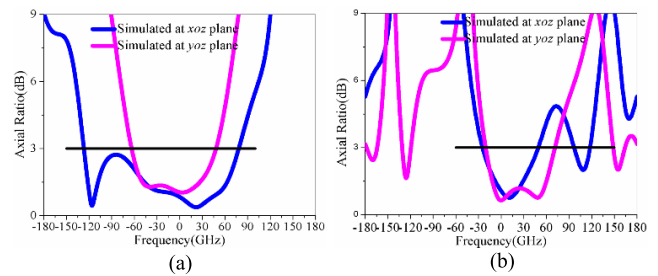
x axis with respect to the slot antenna without an MS. It is noteworthy that the proposed antenna has an average 20-dB RCS reduction in a wide band from 5.25 to 6.8 GHz, which is covered by the PC band.

Figs. 9(a) and 9(b) demonstrate the angular dependence of the AR, for which larger AR beams have been exhibited at sampling frequencies of 5.6 and 6.2 GHz. It can be seen that the simulated AR angular bandwidth of the proposed antenna is $200°$ ($-135°$ to $75°$) and $105°$ ($-30°$ to $45°$ and $90°$ to $120°$) at 5.6 and 6.2 GHz, respectively, in the xoz plane. The corresponding bandwidths are $120°$ ($-60°$ to $60°$) and $105°$ ($-30°$ to $75°$) in the yoz plane at the same two frequencies. For clarity, physical explanations are provided in the following section, owing to the fact that the design exhibits a better PR property than previously published PRSs.

In previous work [21], corner-cut PRS was adopted to realize linear-to-circular polarization, where energy was also coupled to the radiation part by utilizing a slot structure. As is known, a slot structure has been widely used for coupled feeding, owing to its wide impedance and simple design, and it is also adopted in the present work. The magnitudes of the reflection coefficients $\Gamma_{TM/TM}$ and $\Gamma_{TE/TM}$ of corner-cut and dual-patch PRRS are presented in Fig. 3(b). It can be seen that two PR points shift to lower frequencies with respect to the corner-cut PRS, but with little impact on the PR bandwidth, leading to a shift of the center frequency to a lower value. Based on the above analysis, the impedance band will also be adjusted to a lower frequency to achieve CP radiation. Then, compared to two PRSs, the slot antenna, as the coupled feeding structure, can produce almost the same impedance width but with a shift of the center frequency to a lower value. Hence, the profile will be lower, and the electric size will be more compact. Thus, a metallic metamaterial with a connecting ground plane and feed line, as well as a graduated structure, have been adopted in this design to match the lower AR band.

It is noted that the PR bands in previous work [26]–[28] are obviously wider than those of the proposed PCMs, but we are aiming at a PCM-based antenna with properties comparable to those described in recent related work.

III. SIMULATION AND MEASUREMENT RESULTS

According to the improved structural parameters, the antenna prototype was generated and examined. To clearly

TABLE 1. Performance comparison of proposed antenna and recent single-fed wideband CP patch antennas.

| Antenna Type	Overall Antenna Volume(λ_0^3)	Impedance bandwidth	3-dB AR bandwidth	Peak gain (dBic)	3-dB AR beam width	
					xoz	yoz
Proposed	*0.55×0.55×0.05*	*42.7%*	*26.2%*	*6.7*	*200°*	*120°*
Ref. [11]	0.32×0.32×0.032	16%	10%	>5.5dBi	116.8°	33.5°
Ref. [21]	0.75×0.73×0.09	32%	20%	About 7	Not given	Not given
Ref. [22]	0.86×0.86×0.04	16.8%	18%	6.8	208°	75°
Ref. [23]	1.23×1.23×0.07	5.6%	5.6%	Not given	30°	30°
Ref. [24]	1.2×1.2×0.95	48.6%	20.4%	approx. 6	Not given	Not given
Ref. [25]	0.58×0.58×0.056	45.6%	23.4%	7.6	Not given	Not given
Ref. [29]	0.3×0.3×0.06	110.3%	54.1%	4.3	Not given	Not given
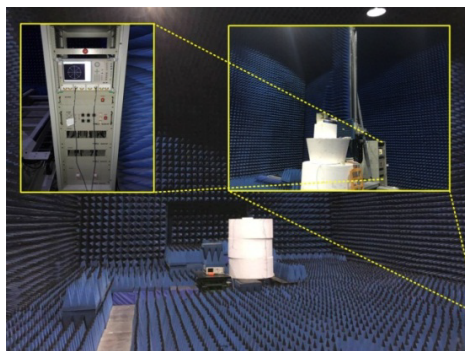
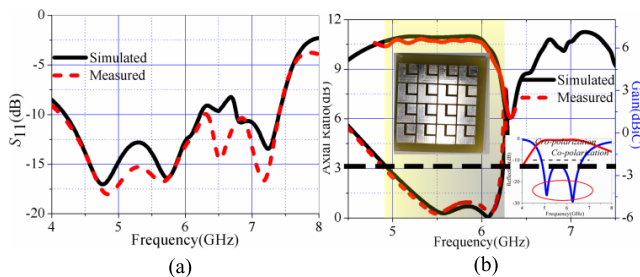
FIGURE 10. Measurement environment in microwave anechoic chamber.

FIGURE 11. Simulated and quantified outcomes of suggested antenna: (a) $|S_{11}|$ and (b) RHCP radiation gain and AR.

FIGURE 12. (a) Simulated beam widths of PCM-based antenna, AR < 3 dB in xoz and yoz planes; (b) Simulated and measured ARs vs. elevation angle of PRRS-based dipole antenna at 5.67 GHz.

FIGURE 13. Radiation patterns of simulation and measurements at 5.4 GHz in (a) xoz and (b) yoz planes.

demonstrate the measurement process, a photograph of the measurement environment in a microwave anechoic chamber is shown in Fig. 10. As depicted in Fig. 11(a), the proposed antenna has a measured 10-dB bandwidth of 2.25 GHz (4.15-6.4 GHz) and 3-dB AR bandwidth of 1.45 GHz (4.8-6.25 GHz), which agree satisfactorily with the simulated results and also correspond with the PR band. The antenna's S_{11} parameters were quantified with a vector network analyzer (Agilent E8361A). The RHCP and LHCP radiation patterns and AR were measured in an anechoic chamber using a standard-gain horn antenna as a reference, and computed using data from their far-field components with formulae from the literature [12].

Further, as seen in Fig. 11(b), the peak LHCP radiation gain on the z axis inside the AR band is 6.7 dB (attained at 6 GHz), with a 0.5-dB degradation in the simulated outcomes. As shown in Fig. 12(a), the beam widths for AR < 3 dB with frequencies in both the xoz and yoz planes were investigated. Fig. 12(b) shows that the frequency in
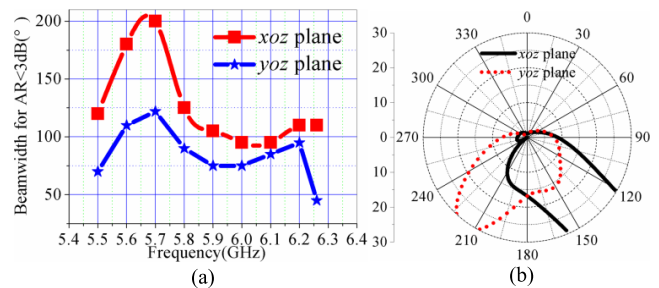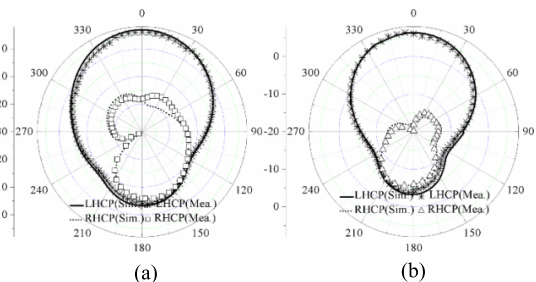
the operational band of the largest beam widths occurred at 5.67 GHz, which can reach 200° in the xoz plane and 120° in the yoz plane. This can be explained by consistent frequency responses under oblique incident waves within the operational band, as demonstrated in Fig. 8(b). The proposed antenna exhibits better AR properties, especially the AR beam width. As revealed in Figs. 13(a) and (b), the suggested antenna yielded good broadside LHCP radiation with good cross-polarizations beneath 25 dB within the bandwidth of CP operation in the two planes. As listed in Table I, compared with recent related work, the proposed antenna exhibited a better CP property, wider AR bandwidth, wider 3-dB AR beam width, and low profile. With good performance and a basic structure, the suggested antenna can be used on the C (4-8 GHz) bands.

IV. CONCLUSIONS
We have shown a broad bandwidth, wide 3-dB AR beam width, and low-profile CP slot antenna utilizing a polarization

conversion according to a dual-patch MS. Through theoretical evaluation, numerical optimizations, and parametric research, the dual-patch-based PCM antenna exhibited a simulated impedance bandwidth of 2.25 GHz (4.15-6.4 GHz) and a 3-dB axial-ratio bandwidth of 1.45 GHz (4.8-6.25 GHz) centered at 5.275 GHz and validated by measurements. The proposed antenna exhibits a better AR property, especially the 3-dB AR beam width within the CP operational bandwidth, than in recent related work. The suggested antenna produced a good RHCP with a peak broadside advantage of 6.7 dB. Owing to its better AR property, this PCM-based antenna has valuable applications for the C band, such as stealth aircraft and satellite communication systems.

REFERENCES

[1] J. Zhu and G. V. Eleftheriades, "A compact transmission-line metamaterial antenna with extended bandwidth," *IEEE Antennas Wireless Propag. Lett.*, vol. 8, pp. 295–298, 2009.

[2] C. L. Holloway, E. F. Kuester, J. A. Gordon, J. O'Hara, J. Booth, and D. R. Smith, "An overview of the theory and applications of metasurfaces: The two-dimensional equivalents of metamaterials," *IEEE Antennas Propag. Mag.*, vol. 54, no. 2, pp. 10–35, Apr. 2012.

[3] B. Ratni, A. de Lustrac, S. Villers, and S. N. Burokur, "Low-profile circularly polarized fabry–perot cavity antenna," *Microw. Opt. Technol. Lett.*, vol. 58, no. 12, pp. 2957–2960, 2016.

[4] R. Orr, G. Goussetis, and V. Fusco, "Design method for circularly polarized fabry–perot cavity antennas," *IEEE Trans. Antennas Propag.*, vol. 62, no. 1, pp. 19–26, Jan. 2014.

[5] M. G. Silveirinha, "Design of linear-to-circular polarization transformers made of long densely packed metallic helices," *IEEE Trans. Antennas Propag.*, vol. 56, no. 2, pp. 390–401, Feb. 2008.

[6] Y. Jia, Y. Liu, and S. Gong, "Wideband high-gain circularly polarized planar antenna based on polarization rotator," in *Proc. Int. Conf. Electromagn. Adv. Appl. (ICEAA)*, Cairns, QLD, Australia, Sep. 2016, pp. 416–419.

[7] J. Y. Chin, M. Lu, and T. J. Cui, "Metamaterial polarizers by electric-field-coupled resonators," *Appl. Phys. Lett.*, vol. 93, no. 25, p. 251903, 2008.

[8] X. Ma *et al.*, "Multi-band circular polarizer using planar spiral metamaterial structure," *Opt. Express*, vol. 20, no. 14, pp. 16050–16058, 2012.

[9] M. Mutlu, A. E. Akosman, A. E. Serebryannikov, and E. Ozbay, "Asymmetric chiral metamaterial circular polarizer based on four U-shaped split ring resonators," *Opt. Lett.*, vol. 36, no. 9, pp. 1653–1655, 2011.

[10] S. V. Pushpakaran *et al.*, "An experimental verification of metamaterial coupled enhanced transmission for antenna applications," *Appl. Phys. Lett.*, vol. 104, no. 6, p. 064102, 2014.

[11] T. Yue, Z. H. Jiang, and D. H. Werner, "Compact, wideband antennas enabled by interdigitated capacitor-loaded metasurfaces," *IEEE Trans. Antennas Propag.*, vol. 64, no. 5, pp. 1595–1606, May 2016.

[12] Z. Wu, L. Li, Y. Li, and X. Chen, "Metasurface superstrate antenna with wideband circular polarization for satellite communication application," *IEEE Antennas Wireless Propag. Lett.*, vol. 15, pp. 374–377, 2016.

[13] Q. Zheng, C. Guo, and J. Ding, "Wideband and low RCS circularly polarized slot antenna based on polarization conversion of metasurface for satellite communication application," *Microw. Opt. Technol. Lett.*, vol. 60, no. 3, pp. 679–685, 2018.

[14] Q. Zheng, C. Guo, and J. Ding, "Wideband and low RCS planar circularly polarized array based on polarization conversion of metasurface," *Microw. Opt. Technol. Lett.*, vol. 60, no. 3, pp. 784–789, 2018.

[15] H. L. Zhu, S. W. Cheung, K. L. Chung, and T. I. Yuk, "Linear-to-circular polarization conversion using metasurface," *IEEE Trans. Antennas Propag.*, vol. 61, no. 9, pp. 4615–4623, Sep. 2013.

[16] H. L. Zhu, S. W. Cheung, X. H. Liu, and T. I. Yuk, "Design of polarization reconfigurable antenna using metasurface," *IEEE Trans. Antennas Propag.*, vol. 62, no. 6, pp. 2891–2898, Jun. 2014.

[17] L. Zhang and T. Dong, "Low RCS and high-gain CP microstrip antenna using SA-MS," *Electron. Lett.*, vol. 53, no. 6, pp. 375–376, 2017.

[18] Y. Jia, Y. Liu, H. Wang, K. Li, and S. Gong, "Low-RCS, high-gain, and wideband mushroom antenna," *IEEE Antennas Wireless Propag. Lett.*, vol. 14, pp. 277–280, 2015.

[19] Y. Jia, Y. Liu, S. Gong, W. Zhang, and G. Liao, "A low-RCS and high-gain circularly polarized antenna with a low profile," *IEEE Antennas Wireless Propag. Lett.*, vol. 16, pp. 2447–2480, 2017.

[20] H. Jiang, Z. Xue, Q. Zeng, W. Li, and W. Ren, "High-gain low-RCS slot antenna array based on checkerboard surface," *IET Microw., Antennas Propag.*, vol. 12, no. 2, pp. 237–240, 2018.

[21] Y. Huang, L. Yang, J. Li, Y. Wang, and G. Wen, "Polarization conversion of metasurface for the application of wide band low-profile circular polarization slot antenna," *Appl. Phys. Lett.*, vol. 109, no. 5, p. 054101, 2016.

[22] W. Yang, K.-W. Tam, W.-W. Choi, W. Che, and H. T. Hui, "Novel polarization rotation technique based on an artificial magnetic conductor and its application in a low-profile circular polarization antenna," *IEEE Trans. Antennas Propag.*, vol. 62, no. 12, pp. 6206–6216, Dec. 2014.

[23] F. Yang and Y. Rahmat-Samii, "A low profile single dipole antenna radiating circularly polarized waves," *IEEE Trans. Antennas Propag.*, vol. 53, no. 9, pp. 3083–3086, Sep. 2005.

[24] T. Nakamura and T. Fukusako, "Broadband design of circularly polarized microstrip patch antenna using artificial ground structure with rectangular unit cells," *IEEE Trans. Antennas Propag.*, vol. 59, no. 6, pp. 2103–2110, Jun. 2011.

[25] S. X. Ta and I. Park, "Low-profile broadband circularly polarized patch antenna using metasurface," *IEEE Trans. Antennas Propag.*, vol. 63, no. 12, pp. 5929–5934, Dec. 2015.

[26] Y. Jia, Y. Liu, W. Zhang, and S. Gong, "Ultra-wideband and high-efficiency polarization rotator based on metasurface," *Appl. Phys. Lett.*, vol. 109, no. 5, p. 051901, Aug. 2016.

[27] Y. Jia, Y. Liu, Y. J. Guo, K. Li, and S. Gong, "A dual-patch polarization rotation reflective surface and its application to ultra-wideband RCS reduction," *IEEE Trans. Antennas Propag.*, vol. 65, no. 6, pp. 3291–3295, Jun. 2017.

[28] Y. Jia, Y. Liu, Y. J. Guo, K. Li, and S.-X. Gong, "Broadband polarization rotation reflective surfaces and their application on RCS reduction," *IEEE Trans. Antennas Propag.*, vol. 64, no. 1, pp. 179–188, Jan. 2016.

[29] M. Nosrati and N. Tavassolian, "A compact circularly-polarized square slot antenna with enhanced axial-ratio bandwidth using metasurface," in *Proc. IEEE Int. Symp. Antennas Propag. USNC/URSI Nat. Radio Sci. Meeting*, San Diego, CA, USA, Jul. 2017, pp. 107–108.

QIANG CHEN was born in Nanchang, Jiangxi, China. He received the bachelor's and master's degree from Air Force Engineering University, Xi'an, China, in 2011 and 2013, respectively, where he is currently pursuing the Ph.D. degree in electrical science and technology. His research interests include microwave circuits, antennas, and arrays.

HOU ZHANG received the B.S. degree from Xi'an Electronic and Engineering University, the M.S. degree from the Air Force Missile College, and the Ph.D. degree from Xidian University, all in electromagnetic field and microwave technology. He has been the session Chair of PIERS and APEMC. He is currently interested in planar antennas and EMC. He has published over 150 technical papers and authored/edited six books. He is holding 6 granted/filed patents.

• • •